EFFECTIVE DISCRETIZATION OF DIRECT RECONSTRUCTION SCHEMES FOR PHOTOACOUSTIC IMAGING IN SPHERICAL GEOMETRIES

FRANK FILBIR[†], STEFAN KUNIS[‡], AND RUBEN SEYFRIED[§]

Abstract. Recently, kernel methods for the recovery of a function from its spherical means in spherical acquisition geometry have been proposed. We present efficient algorithms for these formulas in the two- and three-dimensional case. Our scheme applies Fourier techniques for certain convolution type integrals and discretizes physical space on a polar and spherical grid, respectively.

Key words and phrases : Radon transform, spherical means, fast Fourier transform.
2010 AMS Mathematics Subject Classification : 44A12, 65R32, 65T50, 92C55.

1. Introduction. Analogously to the inversion of the Radon transform in computerized tomography, recovering a function from its mean values over a family of spheres is relevant in photoacoustic tomography. The spherical mean operator $\mathcal{R} : C(\mathbb{R}^d) \to C(\mathbb{R}^d \times [0,\infty))$ is defined by

$$\mathcal{R}f(\xi,t) = \int_{\mathbb{S}^{d-1}} f(\xi + tu)\ \mathrm{d}\sigma(u), \tag{1.1}$$

where $\mathbb{S}^{d-1} = \left\{u \in \mathbb{R}^d : |u| = 1\right\}$ denotes the unit sphere and σ its surface measure with $\sigma(\mathbb{S}^1) = 2\pi$ and $\sigma(\mathbb{S}^2) = 4\pi$. The variable $t \geq 0$ is called measurement time and the variable $\xi \in \mathbb{R}^d$ detector position or center point. In all practical applications these center points are located on a curve or surface and we consider the classical case $\xi \in \mathbb{S}^{d-1}$ here. Moreover, we restrict ourselves to functions $f : \mathbb{R}^d \to \mathbb{R}$ with support $\mathrm{supp} f \subset \mathbb{B}$, where $\mathbb{B} = \left\{x \in \mathbb{R}^d : |x| < 1\right\}$ denotes the open unit ball, such that the spherical mean values $\mathcal{R}f(\xi,t)$ vanish for $t \geq 2$.

Recovering the function f from the spherical means amounts to an inversion of the operator (1.1). Exact inversion formulae for f were presented in [5, 4, 16, 10, 1, 9]. The focus of the present paper lies on the discretization of approximate inversion methods which were presented in [3, 1], where the function f can be approximated from the spherical mean values $\mathcal{R}f(\xi,t)$, $\xi \in \mathbb{S}^{d-1}$, $t \in [0,2]$, using specific summability kernels. These summability kernels are families of integrable functions $K_\varepsilon : \mathbb{B} \times \mathbb{B} \to \mathbb{R}$, where $\varepsilon \in (0,1)$ is a regularization parameter, with the properties

$$K_\varepsilon(x,y) = \int_{\mathbb{S}^{d-1}} k_\varepsilon(x,\xi,|y-\xi|)\ \mathrm{d}\sigma(\xi),$$
$$f(x) = \lim_{\varepsilon\to 0} \int_{\mathbb{B}} f(y) K_\varepsilon(x,y)\ \mathrm{d}y,$$

and $k_\varepsilon : \mathbb{B} \times \mathbb{S}^{d-1} \times [0,2] \to \mathbb{R}$ denotes some auxiliary function. Then a simple calculation shows, see [1, eq. (3)],

$$f(x) = \lim_{\varepsilon\to 0} \int_0^2 \int_{\mathbb{S}^{d-1}} k_\varepsilon(x,\xi,t) \mathcal{R}f(\xi,t)\ \mathrm{d}\sigma(\xi)\, t^{d-1}\ \mathrm{d}t.$$

Our main objective now is an effective discretization of this reconstruction formula for space dimensions $d = 2$ and $d = 3$. Towards this goal, we integrate over the sphere first

[†]TU München and Helmholtz Zentrum München, frank.filbir@helmholtz-muenchen.de
[‡]University Osnabrück and Helmholtz Zentrum München, stefan.kunis@math.uos.de
[§]Helmholtz Zentrum München, ruben.seyfried@helmholtz-muenchen.de

and understand this step as a convolution for which Fourier techniques are applicable. This is followed by the integration over time and finally, an interpolation step on the reconstruction is performed.

Similar approaches can be found in [11, 8, 14] and references therein. The papers [11, 8] consider approximate reconstruction formulas in $d = 3$ and $d = 2$, respectively. The developed algorithm has three major steps: a filtering step that integrates the data $\mathcal{R}f(\xi, t)$ over time t against a kernel that depends only on the radial coordinate of the reconstruction position, a linear interpolation step on the intermediate data, and a subsequent backprojection step integrating over the sphere. Besides technicalities, this algorithm is efficient since the interpolation step basically decouples radial and angular coordinates. In contrast, our algorithm discretizes physical space on a polar or spherical grid, computes the inner integral of the reconstruction formula efficiently, and interpolates only the final result. In dimension $d = 2$ our algorithm has a complexity of $\mathcal{O}\left(n^{3/2} \log n\right)$ and is therefore slightly slower than conventional implementations of filtered backprojection which has a complexity of $\mathcal{O}\left(n^{3/2}\right)$, see e.g. [4]. In the case $d = 3$ our algorithm needs $\mathcal{O}\left(n^{4/3}\right)$ floating point operations and thus is faster than the implementation of filtered backprojection with $\mathcal{O}\left(n^{5/3}\right)$ floating point operations [11]. Here n denotes the total problem size.

The algorithms in [14] implement exact reconstruction formulas by spectral methods which separate the radial and angular variables. After careful discretization and truncation of involved series, these schemes achieve, up to logarithmic factors, linear arithmetic complexity. The algorithms have four major steps: Fourier transforms with respect to time and also with respect to the angular component, a multiplication step, inverse Fourier transforms with respect to the angular component, an interpolation step from the polar or spherical grid to a Cartesian grid, and a final Fourier transform on the Cartesian grid. In contrast, we implement an *approximate* reconstruction formula and discretize on a polar or spherical in the original domain rather than in the frequency domain. Unfortunately, we do not achieve the almost linear orders in arithmetic complexity, but as pointed out above our algorithms avoids interpolation of intermediate data.

The paper is organized as follows: We consider the two- and the three-dimensional case in Sections 2 and 3, respectively. After introducing the necessary notation, we first present the continuous version of the reconstruction formulas when considered in polar or spherical coordinates. Subsequently, we discretize these formulas on a polar or spherical grid, choose involved parameters and analyze the arithmetic complexity of the obtained algorithms. All theoretical results are illustrated by a couple of numerical experiments in Section 4 and we finally conclude our findings in Section 5.

2. Circular means. For the two-dimensional case $d = 2$, we consider detector positions on the unit circle , i.e. $\xi \in \mathbb{S}^1$, surrounding the support of the function f. For each detector position and measurement time $t \in [0, 2]$, the spherical mean is just the integral of f over a circular arc with midpoint ξ and radius t, see also Figure 2.1(left). An appropriate choice of the function k_ε now is

$$
\begin{aligned}
h : \mathbb{R} \to \mathbb{R}, \qquad & h(t) = \frac{1}{2\pi} \frac{1 - t^2}{(1 + t^2)^2}, \\
h_\varepsilon : [-2, 2] \to \mathbb{R}, \qquad & h_\varepsilon(t) = \frac{1}{\varepsilon^2} h(\frac{t}{\varepsilon}), \\
k_\varepsilon : \mathbb{B} \times \mathbb{S}^1 \times [0, 2] \to \mathbb{R}, \qquad & k_\varepsilon(x, \xi, t) = \frac{2}{\pi}(1 - |x|^2) h_\varepsilon(|x - \xi|^2 - t^2).
\end{aligned}
$$

The result that this indeed produces a summability kernel is given in [1, Corollary 2, Section (3.2)]. As a consequence we get an approximation to the function f by

$$f_\varepsilon(x) = \frac{2}{\pi}(1-|x|^2)\int_0^2 \int_{\mathbb{S}^1} h_\varepsilon(|x-\xi|^2 - t^2)\mathcal{R}f(\xi,t)\,\mathrm{d}\sigma(\xi)\,t\,\mathrm{d}t. \tag{2.1}$$

We show that this reconstruction can be understood as a convolution when we use polar coordinates for the function f. Discretization leads to a polar grid as depicted in Figure 2.1(middle) and a bilinear interpolation on each polar wedge, cf. Figure 2.1(right) finally gives the reconstruction of f on a Cartesian grid.

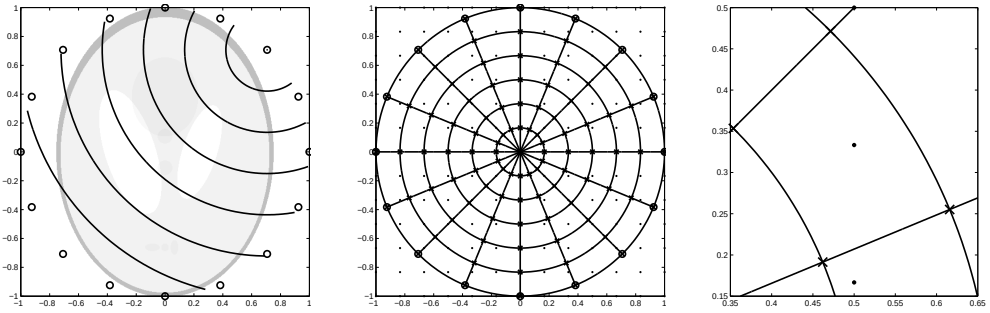

Fig. 2.1: Measurement and reconstruction geometry.

Using the standard parameterization $\xi = (\cos\psi, \sin\psi)^\top$, $\psi \in [0, 2\pi)$, of the circle $\mathbb{S}^1$ and expressing $x \in \mathbb{B}$ in polar coordinates $x = r(\cos\varphi, \sin\varphi)^\top$, $r \in [0,1)$, $\varphi \in [0, 2\pi)$, yields

$$|x-\xi|^2 = 1 + r^2 - 2r\cos(\psi - \varphi).$$

For notational convenience, we denote fixed arguments of functions as superscript and skipping the parameter ε completely, i.e.,

$$\begin{aligned} h^{r,t}(\psi) &= h_\varepsilon(1 + r^2 - 2r\cos\psi - t^2), \\ g^t(\psi) &= t \cdot \mathcal{R}f\left(\cos\psi, \sin\psi, t\right), \end{aligned}$$

Hence, the approximation (2.1) can be written as a periodic convolution with respect to the angular component

$$\begin{aligned} f^{r,t}(\varphi) &= \left(h^{r,t} * g^t\right)(\varphi) = \int_0^{2\pi} h^{r,t}(\varphi - \psi) g^t(\psi)\,\mathrm{d}\psi, \\ f_\varepsilon\left(r\cos\varphi, r\sin\varphi\right) &= \frac{2}{\pi}(1-r^2)\int_0^2 f^{r,t}(\varphi)\,\mathrm{d}t. \end{aligned}$$

Typically, the measurement times $t \in [0,2]$ are equidistant and the detector positions are equiangular $\xi_n = (\cos\psi_n, \sin\psi_n)^\top \in \mathbb{S}^1$,

$$\begin{aligned} t_m &= \frac{2m}{M}, & m &= 0, \ldots, M-1, \\ \psi_n &= \frac{2\pi n}{N}, & n &= 0, \ldots, N-1. \end{aligned}$$

Thus, the integrals in (2.1) are discretized via composite quadrature rules with equidistant nodes. In the angular variable, constant weights give the highest trigonometric degree of exactness, in the time variable, constant weights yield a midpoint rule. We discretize the spatial variable x accordingly on a polar grid $x_{\ell,j} = r_j(\cos\varphi_\ell, \sin\varphi_\ell)^\top$,

$$\begin{aligned} r_j &= \frac{j}{J}, & j &= 0, \dots, J-1, \\ \varphi_\ell &= \frac{2\pi\ell}{N}, & \ell &= 0, \dots, N-1, \end{aligned}$$

which leads for fixed $\varepsilon \in (0,1)$ to the discrete reconstruction formula

$$\begin{aligned} f_\varepsilon(x_{\ell,j}) \approx f_\ell^j &:= \frac{8(1-|x_{\ell,j}|^2)}{MN} \sum_{m=0}^{M-1} f_\ell^{j,m} \\ f_\ell^{j,m} &:= \sum_{n=0}^{N-1} h_\varepsilon(1 + r_j^2 - t_m^2 - 2r_j\cos\psi_{n-\ell})\, t_m \cdot \mathcal{R}f(\xi_n, t_m) \end{aligned} \tag{2.2}$$

For fixed indices j, m, the second sum is a multiplication with a circulant matrix, i.e., $\boldsymbol{f}^{j,m} = \boldsymbol{H}^{j,m}\boldsymbol{g}^m$, where

$$\begin{aligned} \boldsymbol{f}^{j,m} &:= (f_\ell^{j,m})_{\ell=0,\dots,N-1} \in \mathbb{R}^N, \\ \boldsymbol{g}^m &:= (t_m \cdot \mathcal{R}f(\xi_n, t_m))_{n=0,\dots,N-1} \in \mathbb{R}^N, \\ \boldsymbol{H}^{j,m} &:= (h_\varepsilon(1 + r_j^2 - t_m^2 - 2r_j\cos\psi_{n-\ell}))_{\ell,n=0,\dots,N-1} \in \mathbb{R}^{N\times N}. \end{aligned}$$

We diagonalize $\boldsymbol{H}^{j,m} = \frac{1}{N}\boldsymbol{F}^* \operatorname{diag} \hat{\boldsymbol{h}}^{j,m} \boldsymbol{F}$ by a discrete Fourier transform, where

$$\begin{aligned} \boldsymbol{F} &:= (\mathrm{e}^{-2\pi \mathrm{i} kn/N})_{k,n=0,\dots,N-1}, \\ \hat{\boldsymbol{h}}^{j,m} &:= \boldsymbol{F}\boldsymbol{h}^{j,m}, \\ \boldsymbol{h}^{j,m} &:= (h_\varepsilon(1 + r_j^2 - t_m^2 - 2r_j\cos\psi_n))_{n=0,\dots,N-1}. \end{aligned}$$

We bring the inverse Fourier transform in front of the outer summation in (2.2) and have the following Algorithm 1.

REMARK 2.1. *Finally, the function f needs to be evaluated on a Cartesian grid and since the reconstruction yields function values on the polar grid, we employ the following interpolation scheme, see also Figure 2.1(middle). Let the discretization parameter $L \in \mathbb{N}$ and nodes $z_{s,t} = (s/L, t/L)$, $s,t = -L, \dots, L$, be given. For ease of notation, consider some fixed node $z_{s,t}$ in the positive quadrant with $\|z_{s,t}\|_2 < 1$, define indices and weights*

$$\begin{aligned} j &= \left\lfloor \frac{J\sqrt{s^2+t^2}}{L} \right\rfloor, & w_{s,t,j} &= J\left(\frac{\sqrt{s^2+t^2}}{L} - r_j\right), \\ \ell &= \left\lfloor \frac{N}{2\pi} \arctan\frac{t}{s} \right\rfloor, & v_{s,t,\ell} &= \frac{N}{2\pi}\left(\arctan\frac{t}{s} - \varphi_\ell\right), \end{aligned}$$

and interpolate bilinearly in the polar grid by

$$\tilde{f}_\varepsilon(z_{s,t}) = (1 - w_{s,t,j})\,(1 - v_{s,t,\ell})\, f_l^j + w_{s,t,j}\,(1 - v_{s,t,\ell})\, f_l^{j+1} \tag{2.3}$$

$$+ (1 - w_{s,t,j})\, v_{s,t,\ell} f_{l+1}^{j} + w_{s,t,j} v_{s,t,\ell} f_{l+1}^{j+1}.$$

Figure 2.1(right) illustrates part of the polar grid and one evaluation node $z_{s,t}$ in its polar wedge. Alternatively, one might use a nearest neighbor interpolation in the polar grid or a constant or linear interpolation over some triangulation of the polar grid.

Algorithm 1

Input : discretization parameter $N, M, J \in \mathbb{N}$,
measurement times $t_m = \frac{2m}{M}$, $m = 0, \ldots, M-1$,
detector positions $\xi_n = (\cos\psi_n, \sin\psi_n)$, $\psi_n = \frac{2\pi n}{N}$, $n = 0, \ldots, N-1$,
data $\mathcal{R}f(\xi_n, t_m)$, $n = 0, \ldots, N-1$, $m = 0, \ldots, M-1$,
radii $r_j = \frac{j}{J}$, $j = 0, \ldots, J-1$,
angles $\varphi_\ell = \frac{2\pi\ell}{N}$, $\ell = 0, \ldots, N-1$.

Output : values $f_l^j \approx f_\varepsilon(r_j \cos\varphi_\ell, r_j \sin\varphi_\ell)$, $\ell = 0, \ldots, N-1$, $j = 0, \ldots, J$.

for $j = 0, \ldots, J-1$ ***do***
  for $m = 0, \ldots, M-1$ ***do***
    set $\boldsymbol{g}^m = (t_m \cdot \mathcal{R}f(\xi_n, t_m))_{n=0,\ldots,N-1}$
    compute $\hat{\boldsymbol{f}}^{j,m} = \mathrm{diag}(\hat{\boldsymbol{h}}^{j,m})\boldsymbol{F}\boldsymbol{g}^m$
  end for
  compute $\hat{\boldsymbol{f}}^j = \frac{8(1-r_j^2)}{MN^2} \sum_{m=0}^{M-1} \hat{\boldsymbol{f}}^{j,m}$
  compute $\boldsymbol{f}^j = \boldsymbol{F}^* \hat{\boldsymbol{f}}^j$
end for

2.1. Parameter choice and computational complexity. An important question concerns the choice of the parameter ε, see also [8, Section 5.1]. While the approximation (2.1) becomes better for smaller ε, the discretization of the outer integral by a composite midpoint rule produces reasonable results only if the integrand is smooth with respect to the mesh size M^{-1} in (2.2). Since the function h_ε has its main lobe in the interval $[-\varepsilon, \varepsilon]$ and a constant number $C \geq 1$ of samples should lie inside this interval, we set

$$\varepsilon = \frac{C}{M},$$

which can further decreased by an artificial increase of the resolution of the measurements, e.g., by interpolation.

The inner sum in (2.2) is a discrete and cyclic convolution and can be realized by means of fast Fourier transforms in $\mathcal{O}(N \log N)$ floating point operations. Taking into account the outer summation over time in (2.2) for all radii, this leads to $\mathcal{O}(JMN \log N)$ floating point operations. Interpolation of the result in (2.3) is a local operation and takes only $\mathcal{O}(JN + L^2)$ floating point operations. Assuming finally $\mathcal{O}(J) = \mathcal{O}(L) = \mathcal{O}(M) = \mathcal{O}(N)$ and considering the total problem size $n = N^2$, our algorithm has complexity $\mathcal{O}(n^{1.5} \log n)$. We note in passing, that the polar grid discretization might be coarsened near the origin saving a fraction of the total computations and that a generalization to nonequally spaced detectors on the unit circle is straightforward using the nonequispaced FFT [13].

3. Spherical means. For the three-dimensional case $d = 3$, we consider detector positions on the unit sphere, i.e. $\xi \in \mathbb{S}^2$, surrounding the support of the function f, see Figure 3.1(left). For each detector position and measurement time $t \in [0, 2]$, the spherical mean is just the integral of f over a spherical cap with midpoint ξ and radius t, see also Figure 3.1(right).

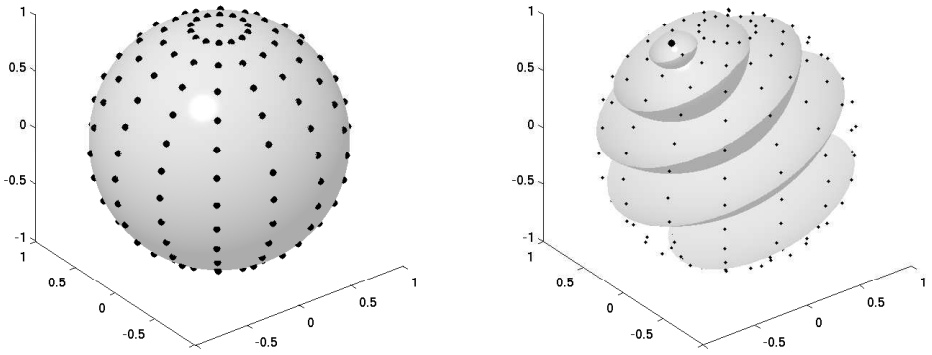

Fig. 3.1: Measurement geometry. Aquisition surface and detector positions (left), spherical shells over which the function is integrated for a single detector (right).

Now the results in [1, Theorem 4, Section (4.2)] give rise to a whole family of reconstruction formulas. Let $q \in \mathbb{N}$, $q \geq 2$, be given and define $c_q = \frac{4\Gamma\left(q+\frac{5}{2}\right)}{\sqrt{\pi}\Gamma(q+1)}$. Let $(t)_+ = \max\{t, 0\}$,

$$\begin{aligned} h_q &: \mathbb{R} \to \mathbb{R}, & h_q(t) &= c_q \left[\left(1-t^2\right)_+^q - 2qt^2 \left(1-t^2\right)_+^{q-1} \right], \\ h_{\varepsilon,q} &: [-2, 2] \to \mathbb{R}, & h_{\varepsilon,q}(t) &= \frac{1}{\varepsilon^3} h_q(\frac{t}{\varepsilon}), \\ k_{\varepsilon,q} &: \mathbb{B} \times \mathbb{S}^2 \times [0, 2] \to \mathbb{R}, & k_{\varepsilon,q}(x, \xi, t) &= \frac{(1-|x|^2)}{2\pi^2} h_{\varepsilon,q}(|x-\xi|^2 - t^2). \end{aligned} \tag{3.1}$$

The conditions of [1, Theorem 4] are satisfied since the function h_q is even, locally integrable, $h_q(t) = c_q \frac{\mathrm{d}}{\mathrm{d}t} t(1-t^2)_+^q$, and the function $H_q : \mathbb{R}^3 \to \mathbb{R}$,

$$H_q(x) := \frac{1}{4\pi} \int_{\mathbb{S}^2} h_q(\langle x, \xi \rangle) \, \mathrm{d}\sigma(\xi) = \frac{1}{|x|} \int_{-|x|}^{|x|} h_q(t) \, \mathrm{d}t = \frac{c_q}{4\pi} (1-|x|^2)_+^q,$$

is a radial, $\int_{\mathbb{R}^3} H_q(x) \, \mathrm{d}x = 1$, and $|H_q(x)| \leq \frac{4^q c_q}{4\pi} (1+|x|)^{-2q}$. Hence, the function f can be approximately reconstructed by

$$f_\varepsilon(x) = \frac{(1-|x|^2)}{2\pi^2} \int_0^2 \int_{\mathbb{S}^2} h_{\varepsilon,q}(|x-\xi|^2 - t^2) \mathcal{R}f(\xi, t) \, \mathrm{d}\sigma(\xi) \, t^2 \, \mathrm{d}t. \tag{3.2}$$

In the following we consider the reconstruction with respect to the regularization parameter ε and fixed $q \geq 2$. We propose a reconstruction scheme generalizing the convolution type ideas. We express the spatial variable in spherical coordinates, cf. Figure

3.2(left), generalize the convolution on the circle $\mathbb{S}^1$ to the sphere $\mathbb{S}^2$, and diagonalize the convolutions by means of appropriate fast spherical Fourier transform. Two other approaches, one based on a discretization in cylinder coordinates, cf. Figure 3.2(right), and another one using the compact support of the function $h_{\varepsilon,q}$, are discussed in Section 3.2.

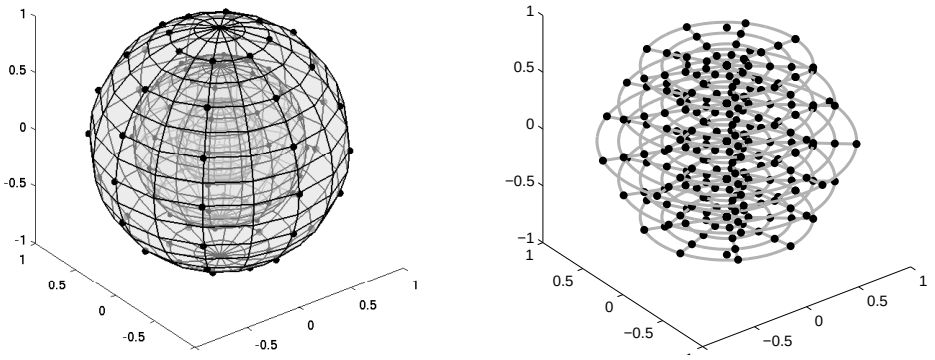

Fig. 3.2: Reconstruction geometries, spherical (left) and cylindrical coordinates (right).

Expressing $x \in \mathbb{B}$ in spherical coordinates $x = r\eta$, $r \in [0,1)$, $\eta \in \mathbb{S}^2$, cf. Figure 3.2(left), yields

$$|x - \xi|^2 = 1 + r^2 - 2r\eta \cdot \xi.$$

We write fixed arguments of functions as superscript and suppress the parameters ε and q completely, i.e.,

$$\begin{aligned} h^{r,t} : [-1,1] \to \mathbb{R}, \qquad & h^{r,t}(y) = h_{\varepsilon,q}(1 + r^2 - t^2 - 2ry), \\ g^t : \mathbb{S}^2 \to \mathbb{R}, \qquad & g^t(\xi) = t^2 \mathcal{R}f(\xi, t), \end{aligned} \tag{3.3}$$

the approximation (3.2) can be written as a convolution of a function on the sphere with a zonal kernel and a subsequent integration

$$\begin{aligned} f^{r,t}(\eta) &= \left(h^{r,t} * g^t\right)(\eta) = \int_{\mathbb{S}^2} h^{r,t}(\eta \cdot \xi) g^t(\xi) \, \mathrm{d}\sigma(\xi), \\ f_\varepsilon(x) &= f_\varepsilon(r\eta) = \frac{(1-r^2)}{2\pi^2} \int_0^2 f^{r,t}(\eta) \, \mathrm{d}t. \end{aligned} \tag{3.4}$$

In order to get a fast algorithm for the convolution (3.4), we follow [12] and expand the function $h^{r,t}$ in a Legendre series. The Legendre-Polynomials $P_k : [-1,1] \to \mathbb{R}$ are defined as

$$P_k(x) = \frac{1}{2^k k!} \frac{\mathrm{d}^k}{\mathrm{d}x^k} \left(x^2 - 1\right)^k,$$

by $Y_k^n : \mathbb{S}^2 \to \mathbb{C}$ we denote the spherical harmonic of degree $k \in \mathbb{N}_0$ and order $n = -k, \ldots, k$. We use the addition theorem for spherical harmonics, which separates

the dependencies of the variables η and ξ in

$$h^{r,t}(\eta \cdot \xi) = \sum_{k=0}^{\infty} \hat{h}_k^{r,t} P_k(\eta \cdot \xi) = \sum_{k=0}^{\infty} \frac{4\pi \hat{h}_k^{r,t}}{2k+1} \sum_{n=-k}^{k} Y_k^n(\eta) \overline{Y_k^n(\xi)}, \tag{3.5}$$

where the Fourier Legendre coefficients are given by

$$\hat{h}_k^{r,t} = \frac{2k+1}{2} \int_{-1}^{1} h^{r,t}(x) P_k(x) \, \mathrm{d}x. \tag{3.6}$$

Since the sum in (3.5) converge absolutely, which follows from Theorem 3.4 below, we can interchange the order of summation and integration, this yields

$$f_\varepsilon(r\eta) = \frac{2}{\pi}(1-r^2) \sum_{k=0}^{\infty} \sum_{n=-k}^{k} Y_k^n(\eta) \int_0^2 \frac{\hat{h}_k^{r,t}}{2k+1} \int_{\mathbb{S}^2} g^t(\xi) \overline{Y_k^n(\xi)} \, \mathrm{d}\sigma(\xi) \, \mathrm{d}t. \tag{3.7}$$

Both integrals are discretized at the locations where the data $\mathcal{R}f(\xi, t)$ is given, i.e., the inner integral at the detector positions and the outer integral at the measurement times

$$\begin{aligned} \xi_i &\in \mathbb{S}^2, & i &= 0, \dots, I^2 - 1, \\ t_m &= \frac{2m}{M}, & m &= 0, \dots, M-1. \end{aligned}$$

We evaluate the function f_ε at points $x_{j,l} = r_j \eta_l$, where

$$\begin{aligned} \eta_l &\in \mathbb{S}^2, & l &= 0, \dots, L^2 - 1, \\ r_j &= \frac{j}{J}, & j &= 0, \dots, J-1. \end{aligned}$$

Moreover, we approximate the series expansion of h^{r_j,t_m} as given in (3.5) at a fixed cut-off degree $N \in \mathbb{N}$ and compute the Fourier coefficients in this series by a quadrature,

$$\hat{h}_k^{r_j,t_m} \approx \hat{h}_k^{j,m} := \sum_{\nu=0}^{N-1} \mu_\nu P_k(\lambda_\nu) h^{r_j,t_m}(\lambda_\nu).$$

Provided $N > 2q$ and the Gauß Legendre nodes and weights (λ_ν, μ_ν) are chosen for the support of $h^{r,t}$, this quadrature is exact since $h^{r,t}$ is a polynomial of degree $2q$ within its support. The resulting truncation error is discussed in Section 3.1.

Our algorithm now works as follows. In a first step and for each measurement time t_m individually, we compute discrete spherical Fourier coefficients

$$\hat{g}_{n,k}^m := \sum_{i=0}^{I^2-1} \omega_i \overline{Y_k^n(\xi_i)} g^{t_m}(\xi_i), \quad k = 0, \dots, N-1, \; n = -k, \dots, k,$$

approximating the inner integral in (3.7) by numerical quadrature on the nodes $\xi_i \in \mathbb{S}^2$ and with some weights $\omega_i > 0$, $i = 0, \dots, I^2 - 1$. These computations are realized via an adjoint nonequispaced fast spherical Fourier transform (adjoint NFSFT), see e.g. [13], the accuracy of this approximation and a precomputation of the weights is discussed in [7].

In a second step and for each radius r_j individually, we compute

$$\hat{f}_{n,k}^j := \frac{2}{M} \sum_{m=0}^{M-1} \frac{\hat{h}_k^{j,m}}{2k+1} \hat{g}_{n,k}^m, \quad k = 0, \dots, N-1,\ n = -k, \dots, k, \tag{3.8}$$

approximating the outer integral in (3.7) by numerical quadrature at the nodes t_m and with constant weights $\frac{2}{M}$. Finally, we evaluate the truncated outer sum in (3.7) at the target nodes η_l, $l = 0, \dots, L^2 - 1$, i.e.,

$$f_\varepsilon(r_j \eta_l) \approx f_l^j := \frac{2(1-r_j^2)}{\pi} \sum_{k=0}^{N} \sum_{n=-k}^{k} \hat{f}_{n,k}^j Y_k^n(\eta_l), \quad l = 0, \dots, L^2 - 1, \tag{3.9}$$

by a nonequispaced fast spherical Fourier transform (NFSFT). For notational convenience, we define

$$\begin{aligned}
\boldsymbol{g}^m &:= \left(\omega_i g^{t_m}(\xi_i)\right)_{i=0,\dots,I^2-1} = \left(\omega_i t_m^2 \mathcal{R} f(\xi_i, t_m)\right)_{i=0,\dots,I^2-1} \in \mathbb{R}^{I^2} \\
\boldsymbol{Y}_\xi &:= \left(Y_k^n(\xi_i)\right)_{i=0,\dots,I^2-1;\ k=0,\dots,N-1,\ n=-k,\dots,k} \in \mathbb{C}^{I^2 \times N^2}, \\
\boldsymbol{Y}_\eta &:= \left(Y_k^n(\eta_l)\right)_{l=0,\dots,L^2-1;\ k=0,\dots,N-1,\ n=-k,\dots,k} \in \mathbb{C}^{L^2 \times N^2}.
\end{aligned}$$

and formulate Algorithm 2.

REMARK 3.1. *The reconstruction yields function values on the spherical grid, see also Figure 3.2(left). Analogously to Remark 2.1, we interpolate trilinear in the spherical grid. We assume $\eta \in \mathbb{S}^2$ is given in the form*

$$\eta_{\ell,n} = \left(\sin(\psi_\ell)\cos(\varphi_n), \sin(\psi_\ell)\sin(\varphi_n), \cos(\psi_\ell)\right)^\top, \qquad \varphi_\ell = \frac{2\pi\ell}{L},\ \psi_n = \frac{\pi n}{L-1},$$

$\ell = 0, \dots, L-1$, $n = 0, \dots, L-1$, and Algorithm 2 outputs values $f_{\ell,n}^j \approx f_\varepsilon(r_j \eta_{\ell,n})$. Let the discretization parameter $K \in \mathbb{N}$ and Cartesian nodes $z_{s,t,w} = \left(\frac{s}{K}, \frac{t}{K}, \frac{p}{K}\right)$, $s,t,p = -K, \dots, K$, be given. For ease of notation, consider some fixed node $z_{s,t,p}$ with $\|z_{s,t,p}\|_2 < 1$ and define the corresponding indices and weights by

$$\begin{aligned}
j &= \left\lfloor \frac{J\sqrt{s^2+t^2+p^2}}{K} \right\rfloor, & w_j &= J\left(\frac{\sqrt{s^2+t^2+p^2}}{K} - r_j\right), \\
\ell &= \left\lfloor \frac{L}{2\pi}\left(\pi + \operatorname{sgn}(t) \operatorname{acos}\frac{s}{\sqrt{s^2+t^2}}\right) \right\rfloor, & v_\ell &= \frac{L}{2\pi}\left(\pi + \operatorname{sgn}(t) \operatorname{acos}\frac{s}{\sqrt{s^2+t^2}} - \varphi_\ell\right), \\
n &= \left\lfloor \frac{L-1}{\pi}\left(\operatorname{acos}\frac{p}{\sqrt{s^2+t^2+p^2}}\right) \right\rfloor, & u_n &= \frac{L-1}{\pi}\left(\operatorname{acos}\frac{p}{\sqrt{s^2+t^2+p^2}} - \psi_n\right).
\end{aligned}$$

Now, interpolate along φ, ψ, and r respectively, by

$$\begin{aligned}
c_{00} &= (1-v_\ell) f_{\ell,n}^j + v_\ell f_{\ell+1,n}^j, & c_{01} &= (1-v_\ell) f_{\ell,n+1}^j + v_\ell f_{\ell+1,n+1}^j, \\
c_{10} &= (1-v_\ell) f_{\ell,n}^{j+1} + v_\ell f_{\ell+1,n}^{j+1}, & c_{11} &= (1-v_\ell) f_{\ell,n+1}^{j+1} + v_\ell f_{\ell+1,n+1}^{j+1}, \\
c_0 &= (1-u_n) c_{00} + u_n c_{01}, & c_1 &= (1-u_n) c_{10} + u_n c_{11}, \\
\tilde{f}_\varepsilon(z_{s,t,p}) &= (1-w_j) c_0 + w_j c_1.
\end{aligned}$$

Algorithm 2

Input : discretization parameter $I, M, L, J, N \in \mathbb{N}$,
measurement times $t_m = \frac{2m}{M}$, $m = 0, \dots, M-1$,
detector positions $\xi_i \in \mathbb{S}^2$, $i = 0, \dots, I^2 - 1$,
data $\mathcal{R}f(\xi_i, t_m)$, $i = 0, \dots, I^2 - 1$, $m = 0, \dots, M-1$
radii $r_j = \frac{j}{J}$, $j = 0, \dots, J-1$,
angles $\eta_l \in \mathbb{S}^2$, $l = 0, \dots, L^2 - 1$.

Output : function values $f_l^j \approx f_\varepsilon(r_j \eta_l)$, $l = 0, \dots, L^2 - 1$, $j = 0, \dots, J-1$.

for $m = 0, \dots, M-1$ ***do***
  set $\boldsymbol{g}^m = \left(\omega_i t_m^2 \mathcal{R}f(\xi_i, t_m)\right)_{i=0,\dots,I^2-1}$
  compute $\hat{\boldsymbol{g}}^m = \boldsymbol{Y}_\xi^* \boldsymbol{g}^m$
end for
for $j = 0, \dots, J-1$ ***do***
  for $k = 0, \dots, N-1$ ***do***
    for $m = 0, \dots, M-1$ ***do***
      compute $\hat{h}_k^{j,m} = \sum_{\nu=0}^{N-1} \mu_\nu P_k(\lambda_\nu) h^{r_j, t_m}(\lambda_\nu)$
    end for
    for $n = -k, \dots, k$ ***do***
      compute $\hat{f}_{n,k}^j = \frac{4(1-r_j^2)}{(2k+1)M\pi} \sum_{m=0}^{M-1} \hat{h}_k^{j,m} \hat{g}_{n,k}^m$
    end for
  end for
  compute $\boldsymbol{f}^j = \boldsymbol{Y}_\eta \hat{\boldsymbol{f}}^j$
end for

3.1. Parameter choice and computational complexity. It remains to choose the parameters $q, N \in \mathbb{N}$, $\varepsilon > 0$, and analyze the final computational complexity of Algorithm 2. Similar to Section 2.1, we argue that the regularization parameter ε is bounded with respect to the discretization of the measurement time, i.e., $\varepsilon \geq CM^{-1}$. Moreover, the parameter $q \in \mathbb{N}$ determines the smoothness of the function $h^{r,t}$ and thus the asymptotic decay of its Fourier Legendre coefficients (3.6). Theorem 3.4 makes this observation precise and allows for an error estimate in Corollary 3.5 which also shows that the asymptotic decay sets in for $k \geq C\varepsilon^{-1}$. Hence, the choice $N = CM$ of the cut-off degree allows for a guaranteed accuracy and a complexity estimate of Algorithm 2.

For notational convenience, we drop all parameters from the considered function $h : \mathbb{R} \to \mathbb{R}$,

$$h(y) := h^{r,t}(y) = h_{\varepsilon,q}(1 + r^2 - t^2 - 2ry).$$

Since

$$\operatorname{supp} h = [v - u, v + u], \quad v := \frac{1 + r^2 - t^2}{2r}, \; u := \frac{\varepsilon}{2r}, \tag{3.10}$$

we obtain that $\operatorname{supp} h \cap [-1, 1] \neq \emptyset$ if and only if

$$t \in \left[\sqrt{((1-r)^2 - \varepsilon)_+}, \sqrt{(1+r)^2 + \varepsilon} \right].$$

Consequently, we have $\hat{h}_k \neq 0$ and thus nonzero terms in the sum (3.8) only if $m = M_1, \dots, M_2$, where

$$M_1 = \left\lceil \frac{M}{2} \sqrt{((1-r_j)^2 - \varepsilon)_+} \right\rceil, \quad M_2 = \min \left\{ \left\lfloor \frac{M}{2} \sqrt{(1+r_j)^2 + \varepsilon} \right\rfloor, M-1 \right\}$$

and this speeds up the total computations. On the other hand, the sum (3.8) represents the integration over t and is a reasonable discretization only if at least a constant number of samples are taken into account. Considering the critical case $r = 0$, dropping the rounding, and using

$$M_2 - M_1 \geq \frac{M}{2} \left(\sqrt{1+\varepsilon} - \sqrt{1-\varepsilon} \right) \geq \frac{M\varepsilon}{2},$$

this is the case for $\varepsilon = C/M$.

We proceed by estimating the Fourier Legendre coefficients (3.6). Trivially, all coefficients fulfill $\hat{h}_k = 0$, $k \in \mathbb{N}_0$, if supp $h \cap [-1,1] = \emptyset$, and we have $\hat{h}_k = 0$, $k \geq 2q+1$, if $[-1,1] \subset$ supp h. We discuss the remaining case and set

$$[a,b] := \text{supp } h \cap [-1,1]. \tag{3.11}$$

We start by bounding the coefficients $\hat{h}_k$ independently of k in Lemma 3.2 and compute the values of the function h and its derivatives in the endpoints of its support in Lemma 3.3. This allows for the estimate on the decay of the Fourier Legendre coefficients $\hat{h}_k$ in Theorem 3.4.

LEMMA 3.2. *The Fourier-Legendre coefficients* (3.6) *satisfy*

$$\left| \hat{h}_k \right| \leq \frac{4q(q+1)c_q}{\varepsilon^3},$$

where c_q is given in (3.1).

Proof. First note, that $h'(a) = h'(b) = 0$ if $-1 < a < b < 1$ and that $P_k(1) = 1$ and $P_k(-1) = (-1)^k$, $k \in \mathbb{N}_0$. In combination with

$$(2k+1)P_k = P'_{k+1} - P'_{k-1}, \quad k \in \mathbb{N}, \tag{3.12}$$

integration by parts leads to

$$\left| \hat{h}_k \right| = \frac{2k+1}{2} \left| \int_a^b h(s) P_k(s) \, \mathrm{d}s \right| \leq \frac{1}{2} \int_a^b |h'(s)| \, |P_{k+1}(s) - P_{k-1}(s)| \, \mathrm{d}s.$$

Using $|P_k(s)| \leq 1$ and

$$\begin{aligned} |h'(s)| &= \frac{2qc_q|(v-s)|}{\varepsilon^3 u^{2q}} (u^2 - (v-s)^2)_+^{q-2} \left| 3u^2 - (2q+1)(v-s)^2 \right| \\ &\leq \frac{4q(q+1)c_q}{\varepsilon^3 u} \leq \frac{8q(q+1)c_q}{\varepsilon^3 (b-a)} \end{aligned}$$

which follows from $\max_{s\in[a,b]} |v-s| \leq \max_{s\in[v-u,v+u]} |v-s| = u$, $(u^2-(v-s)^2)_+ \leq u^2$, and $2u \geq b-a$, the assertion follows. ∎

LEMMA 3.3. *The function h and its derivatives of order $p = 0, \dots, 2q$ satisfy*

$$h^{(p)}(v+u) = \begin{cases} 0 & \text{if } p = 0, \dots, q-2, \\ \frac{(-1)^q 2^{2q-1-p}(p+2)! c_q}{\varepsilon^3 u^p (q+1)} \binom{q+1}{p-q+1} & \text{if } p = q-1, \dots, 2q, \end{cases}$$

and $h^{(p)}(v-u) = (-1)^p h^{(p)}(v+u)$. *See* (3.1) *for the definition of* c_q.

Proof. We consider the auxiliary function $g_q(s) = (u^2 - (v-s)^2)^q = (u-v+s)^q(u+v-s)^q$ which satisfies

$$\begin{aligned} g_q^{(p)}(s) &= \sum_{i=0}^{p} \binom{p}{i} \frac{\mathrm{d}^{p-i}}{\mathrm{d}s^{p-i}}(u-v+s)^q \frac{\mathrm{d}^i}{\mathrm{d}s^i}(u+v-s)^q \\ &= \begin{cases} \sum_{i=0}^{p} \binom{q}{i}\binom{q}{p-i}(-1)^i p!(u-v+s)^{q-p+i}(u+v-s)^{q-i} & \text{if } p<q, \\ \sum_{i=(p-q)}^{q} \binom{q}{i}\binom{q}{p-i}(-1)^i p!(u-v+s)^{q-p+i}(u+v-s)^{q-i} & \text{if } p \geq q, \end{cases} \end{aligned}$$

and as a consequence

$$g_q^{(p)}(v+u) = \begin{cases} 0 & \text{if } p<q, \\ (-1)^q \binom{q}{p-q} p!(2u)^{2q-p} & \text{if } p \geq q. \end{cases}$$

The assertion follows from $g_q^{(p)}(v-u) = (-1)^p g_q^{(p)}(v+u)$ and

$$h(s) = \frac{(2q+1)c_q}{\varepsilon^3} u^{-2q} g_q(s) - \frac{2qc_q}{\varepsilon^3} u^{-2(q-1)} g_{q-1}(s).$$

□

THEOREM 3.4. *The Fourier Legendre coefficients* $\hat{h}_k$ *of the function* h *obey the inequality*

$$\left|\hat{h}_k\right| \leq \frac{C_q\sqrt{u}\left((1-b^2)^{\frac{1}{4}} + (1-a^2)^{\frac{1}{4}}\right)}{\varepsilon^3 \sigma^{q-\frac{1}{2}}} \left(2 + \frac{1}{\sigma}\right)^{q+1}, \quad k > 2q+1,$$

where $a < b$ *are given by* (3.11), $\sigma = u(k-2q)$, $C_q = (2q+1)!c_q$, *and* c_q *is given in* (3.1).

Proof. For notational convenience let $[f]_a^b := f(b) - f(a)$. Induction over $p = 1, \ldots, 2q$, using integration by parts together with equation (3.12), yields

$$\begin{aligned} |\hat{h}_k| &\leq \frac{1}{2} \sum_{i=0}^{p-1} \frac{1}{2^i(k-(p-1))^i} \sum_{l=0}^{i} \binom{i}{l} \left| \left[h^{(i)}(P_{k-i+2l+1} - P_{k-i+2l-1}) \right]_a^b \right| \\ &\quad + \frac{1}{2} \frac{1}{2^{p-1}(k-(p-1))^{p-1}} \sum_{l=0}^{p} \binom{p}{l} \left| \int_a^b h^{(p)}(s) P_{k-p+2l}(s)\, \mathrm{d}s \right| \\ &\leq \frac{1}{2} \sum_{i=0}^{2q} \frac{1}{(2(k-2q))^i} \sum_{l=0}^{i} \binom{i}{l} \left| \left[h^{(i)}(P_{k-i+2l+1} - P_{k-i+2l-1}) \right]_a^b \right|, \end{aligned} \tag{3.13}$$

where the last step for $p = 2q$ is due to $h_q^{(2q)}$ being constant. We use the inequality

$$|P_{k+1}(x) - P_{k-1}(x)| \leq \frac{2(1-x^2)^{\frac{1}{4}}}{\sqrt{k}}, \quad k \geq 2,\ x \in [-1,1],$$

see [2] and [18, p. 172, eq. (7.33.10)] for a related asymptotic statement. Since $[a,b] \subsetneq [-1,1]$, we assume that $b < 1$.Together with the symmetry of the derivatives, this provides

$$\left| \left[h^{(i)}(P_{k-i+2l+1} - P_{k-i+2l-1}) \right]_a^b \right| \leq \left| h^{(i)}(b) \right| \frac{2(1-b^2)^{\frac{1}{4}}}{\sqrt{k-i+2l}} + \left| h^{(i)}(a) \right| \frac{2(1-a^2)^{\frac{1}{4}}}{\sqrt{k-i+2l}}$$

$$\leq \frac{2\left|h^{(i)}(b)\right|}{\sqrt{k-i}}\left((1-b^2)^{\frac{1}{4}}+(1-a^2)^{\frac{1}{4}}\right),$$

where the corresponding term on the right hand side vanishes if $a=-1$. We proceed in (3.13) by

$$\begin{aligned}\left|\hat{h}_k\right| &\leq \sum_{i=0}^{2q}\frac{(1-b^2)^{\frac{1}{4}}+(1-a^2)^{\frac{1}{4}}}{(2(k-2q))^i}\frac{\left|h^{(i)}(b)\right|}{\sqrt{k-i}}\sum_{l=0}^{i}\binom{i}{l}\\ &= \left((1-b^2)^{\frac{1}{4}}+(1-a^2)^{\frac{1}{4}}\right)\sum_{i=0}^{2q}\frac{1}{(k-2q)^i}\frac{\left|h^{(i)}(b)\right|}{\sqrt{k-i}}.\end{aligned}$$

Applying Lemma 3.3, we get

$$\begin{aligned}\sum_{i=0}^{2q}\frac{1}{(k-2q)^i}\frac{\left|h^{(i)}(b)\right|}{\sqrt{k-i}} &\leq \frac{c_q}{\varepsilon^3}\sum_{i=q-1}^{2q}\frac{2^{2q-1-i}}{(k-2q)^{i+\frac{1}{2}}u^i}\binom{q+1}{i-q+1}\frac{(i+2)!}{q+1}\\ &\leq \frac{c_q(2q+1)!}{\varepsilon^3}\sum_{i=q-1}^{2q}\frac{2^{2q-i}}{(k-2q)^{i+\frac{1}{2}}u^i}\binom{q+1}{i-q+1}\\ &= \frac{c_q(2q+1)!\sqrt{u}}{\varepsilon^3\sigma^{q-\frac{1}{2}}}\sum_{i=0}^{q+1}\frac{2^{q+1-i}}{\sigma^i}\binom{q+1}{i}\end{aligned}$$

and the assertion follows by the binomial theorem. □

Corollary 3.5. *Let $\varepsilon\in(0,1)$, $N\in\mathbb{N}$, $N\geq 2/\varepsilon$, and the approximation f_ε in (3.7) be truncated by $f_\varepsilon^N:\mathbb{B}\to\mathbb{R}$,*

$$f_\varepsilon^N(r\eta)=\frac{(1-r^2)}{2\pi^2}\int_0^2\int_{\mathbb{S}^2}h^N(\eta\xi)g^t(\xi)\,\mathrm{d}\sigma(\xi)\,\mathrm{d}t,\quad h^N=\sum_{k=0}^{N+2q-1}\hat{h}_kP_k,$$

where $r\in(0,1)$ and $\eta\in\mathbb{S}^2$, then

$$\|f_\varepsilon-f_\varepsilon^N\|_\infty\leq\frac{\tilde{C}_q(1-r^2)r^{q-1}}{\varepsilon^{\frac{7}{2}}}(\varepsilon N)^{\frac{3}{2}-q}\|f\|_\infty,$$

where $\tilde{C}_q=32\cdot 6^{q+1}\cdot C_q$.

Proof. Using $\max_{x\in[-1,1]}|P_k(x)|=1$, we get

$$\begin{aligned}|f_\varepsilon(r\eta)-f_\varepsilon^N(r\eta)| &\leq \frac{1-r^2}{2\pi^2}\int_0^2\int_{\mathbb{S}^2}\left|h(\eta\xi)-h^N(\eta\xi)\right|\left|g^t(\xi)\right|\,\mathrm{d}\sigma(\xi)\,\mathrm{d}t\\ &\leq \frac{1-r^2}{2\pi^2}\sum_{k=N+2q}^{\infty}|\hat{h}_k|\int_0^2\int_{\mathbb{S}^2}\int_{\mathbb{S}^2}|f(\xi+tu)|\,|t|^2\,\mathrm{d}\sigma(u)\,\mathrm{d}\sigma(\xi)\,\mathrm{d}t\\ &\leq \frac{2^6(1-r^2)}{3}\|f\|_\infty\sum_{k=N+2q}^{\infty}|\hat{h}_k|.\end{aligned}$$

Applying Theorem 3.4 together with $2+\frac{1}{\sigma}\leq 3$ and $u=\frac{\varepsilon}{2r}$, the sum of the Fourier Legendre coefficients is bounded by

$$\sum_{k=N+2q}^{\infty}|\hat{h}_k|\leq\frac{2\,3^{q+1}C_q}{\varepsilon^3u^{q-1}}\sum_{k=N}^{\infty}k^{\frac{1}{2}-q}$$

$$\leq \frac{2\ 3^{q+1}C_q}{\varepsilon^3 u^{q-1}}\left(N^{\frac{1}{2}-q}+\int_N^\infty x^{\frac{1}{2}-q}\,\mathrm{d}x\right)\leq \frac{2\ 3^{q+2}C_q(2r)^{q-1}}{\varepsilon^{\frac{7}{2}}(\varepsilon N)^{q-\frac{3}{2}}}.$$

□

The constants in the above estimate are not optimized in any way and numerical experiments suggest that the actual error includes an additional factor $N^{-\frac{1}{2}}$. In total, the truncation error decays algebraically with a rate depending on the smoothness parameter q and this behavior sets in for $N \geq \varepsilon^{-1}$.

REMARK 3.6. *Regarding the total accuracy of Algorithm 2, we note the following.*

1. *Approximating the function f by* (3.2) *induces the approximation error $\|f - f_\varepsilon\|_\infty$. Based on the summability method presented in [1]. This error can be estimated as*

$$\|f - f_\varepsilon\|_\infty \leq c\omega_\infty(f,\varepsilon) + \sup_{x\in\mathbb{B}} |c_\varepsilon(x) - 1|\,\|f\|_\infty .$$

Here $\omega_\infty(f,\varepsilon) = \sup_{|y|\leq\varepsilon}\|\Delta_y f\|_\infty$ is the modulus of continuity, $\Delta_y f(x) = f(x-y)-f(x)$, and $c_\epsilon(x) = \int_{\mathbb{B}} K_\varepsilon(x,y)\,\mathrm{d}y$ is the normalization of the summability kernel

$$K_\varepsilon(x,y) = \frac{(1-|x|^2)}{2\pi^2}\int_{\mathbb{S}^2} h_\varepsilon\left(\frac{|x-\xi|^2-|y-\xi|^2}{\varepsilon}\right)\mathrm{d}\sigma(\xi),$$

which fulfills $\lim_{\varepsilon\to 0} c_\varepsilon(x) = 1$ for all $x \in \mathbb{B}$. Thus for a detailed convergence statement, one either has to know how fast the integral over the summability kernel $K_\varepsilon(x,y)$ converges to one or one has to normalize the kernel for all ε and x. The error estimation of the two dimensional case (2.1) *with the corresponding summability kernel can be treated similarly. For details of the degree of approximation we refer to [17, Section 3.4].*

2. *Corollary 3.5 discusses the truncation error*

$$\|f_\varepsilon - f_\varepsilon^N\|_\infty$$

and suggests a choice of the truncation parameter N with respect to ε.

3. *Finally, the discrete spherical Fourier coefficients $\hat{g}_{k,n}^m$ of the given data are computed by a quadrature rule. Together with the discretization of the integral over the measurement time, this introduces a discretization error*

$$\max_{j,l} |f_\varepsilon^N(r_j\eta_l) - f_j^l|.$$

Provided the detector positions are somewhat uniformly distributed on the sphere, we expect a degree of exactness $N \approx I$ and a rate of convergence $N^{-q'}$ where q' is related to the smoothness of the given data, see also [7]. The integral over the measurement time is computed by a simple trapezoidal rule whose accuracy is discussed e.g. in [19].

The above discussion supports the parameter choice $\varepsilon = \mathcal{O}(1/M)$, $N = \mathcal{O}(M)$, and moreover, we assume $\mathcal{O}(I) = \mathcal{O}(J) = \mathcal{O}(N)$. Each spherical Fourier transforms in Algorithm 2 is computed in $\mathcal{O}(N^2\log^2 N)$ floating point operations and thus, the most time consuming parts rely on the two innermost loops. Hence, we have a total complexity of $\mathcal{O}(n^{\frac{4}{3}})$ floating point operations with respect to the total problem size $n = N^3$.

3.2. Alternative discretisation strategies. We briefly discuss two other approaches to discretize the reconstruction formula (3.2). Using the compact support of the function $h_{\varepsilon,q}$ and after changing the order of integration, we obtain

$$f_\varepsilon(x) = \frac{(1-|x|^2)}{2\pi^2} \int_{\mathbb{S}^2} \int_{\sqrt{(|x-\xi|^2-\varepsilon)_+}}^{\min\{2,\sqrt{|x-\xi|^2+\varepsilon}\}} h_{\varepsilon,q}(|x-\xi|^2 - t^2) \mathcal{R}f(\xi,t)\, t^2 \, \mathrm{d}t \, \mathrm{d}\sigma(\xi).$$

For simplicity, we consider the case of a single discretization parameter $N \in \mathbb{N}$ and reconstruct f on the Cartesian grid $x_{\ell,p,j} = \frac{1}{N^3}(\ell,p,j)^\top \in [-1,1]^3$, $\ell,p,j = -N,\dots,N$. Discretizing the outer integral by N^2 nodes on $\mathbb{S}^2$ and the inner integral over the original interval $[0,2]$ by N nodes leads for fixed indices l,p,j to

$$f_\varepsilon(x_{l,p,j}) \approx \frac{2c_q(1-|x_{l,p,j}|^2)}{N^3} \sum_{i,n=1}^{N} \sum_{m=N_1}^{N_2} h_{\varepsilon,q}(|x_{l,p,j}-\xi_{i,n}|^2 - t_m^2) \mathcal{R}f(\xi_{i,n},t_m)\, t_m^2 \sin\psi_{1,i}.$$

In case $|x_{l,p,j}-\xi_{i,n}|^2 \geq \varepsilon$, we have

$$\begin{aligned}
(N_2-N_1)^2 &\leq N^2 \left(\sqrt{|x_{l,p,j}-\xi_{i,n}|^2+\varepsilon} - \sqrt{|x_{l,p,j}-\xi_{i,n}|^2-\varepsilon} \right)^2 \\
&= 2N^2 \left(|x_{l,p,j}-\xi_{i,n}|^2 - \sqrt{|x_{l,p,j}-\xi_{i,n}|^4-\varepsilon^2} \right) \\
&\leq 2N^2 \left(|x_{l,p,j}-\xi_{i,n}|^2 - \sqrt{(|x_{l,p,j}-\xi_{i,n}|^2-\varepsilon)^2} \right) = 2\varepsilon N^2,
\end{aligned}$$

in case $|x_{l,p,j}-\xi_{i,n}|^2 < \varepsilon$ even simpler $N_2 - N_1 \leq N\sqrt{|x_{l,p,j}-\xi_{i,n}|^2+\varepsilon} \leq \sqrt{2\varepsilon}N$. Assuming as above $\varepsilon = CN^{-1}$, this yields $N_2 - N_1 = \mathcal{O}(\sqrt{N})$ and thus, with respect to the total problem size $n = N^3$, a total complexity of $\mathcal{O}(n^{\frac{11}{6}})$ floating point operations.

The second approach is a direct generalization of the two-dimensional case, where we express the spatial variable in cylinder coordinates and thus reconstructs f for each fixed third Cartesian coordinate separately, cf. Figure 3.2(right). We use the parameterization $\xi = (\sin\psi_1\cos\psi_2, \sin\psi_1\sin\psi_2, \cos\psi_1)^\top$, $\psi_1 \in [0,\pi]$, $\psi_2 \in [0,2\pi)$, of the sphere $\mathbb{S}^2$ and express $x \in \mathbb{B}$ in cylindrical coordinates $x = (r\cos\varphi, r\sin\varphi, z)^\top$, $r \in [0,1)$, $z \in (-1,1)$, $\varphi \in [0,2\pi)$, which yields

$$|x-\xi|^2 = 1 + r^2 + z^2 - 2r\sin\psi_1\cos(\psi_2-\varphi) - 2z\cos\psi_1.$$

Denoting fixed arguments of functions as superscript and skipping the parameters ε and q completely, i.e.,

$$\begin{aligned}
h^{r,t,z,\psi_1}(\psi_2) &= h_{\varepsilon,q}(1+r^2+z^2-2r\sin\psi_1\cos(\psi_2)-2z\cos\psi_1-t^2), \\
g^{t,\psi_1}(\psi_2) &= t^2 \cdot \mathcal{R}f(\sin\psi_1\cos\psi_2, \sin\psi_1\sin\psi_2, \cos\psi_1, t),
\end{aligned}$$

the approximation (3.2) can be written as a periodic convolution with respect to the angular component

$$\begin{aligned}
f^{r,t,\psi_1,z}(\varphi) &= \left(h^{r,t,\psi_1,z} * g^{\psi_1,t}\right)(\varphi) = \int_0^{2\pi} h^{r,t,\psi_1,z}(\varphi-\psi_2) g^{t,\psi_1}(\psi_2)\, \mathrm{d}\psi_2, \\
f_\varepsilon(r\cos\varphi, r\sin\varphi, z) &= \frac{1}{2\pi^2}(1-r^2-z^2) \int_0^2 \int_0^\pi f^{r,t,\psi_1,z}(\varphi) \sin\psi_1 \, \mathrm{d}\psi_1 \, \mathrm{d}t.
\end{aligned}$$

We assume, as in the two-dimensional case, equidistant measurement times $t \in [0,2]$ and equiangular detector positions $\xi_{i,n} = (\sin\psi_{1,i}\cos\psi_{2,n}, \sin\psi_{1,i}\sin\psi_{2,n}, \cos\psi_{1,i})^\top \in \mathbb{S}^2$,

$$\begin{aligned} t_m &= \frac{2m}{M}, && m = 0,\dots,M-1,\\ \psi_{1,i} &= \frac{\pi i}{I-1}, && i = 0,\dots,I-1,\\ \psi_{2,n} &= \frac{2\pi n}{N}, && n = 0,\dots,N-1. \end{aligned}$$

Furthermore, we discretize the spatial variable $x \in \mathbb{B}$ in cylindrical coordinates $x_{\ell,p,j} = (r_j\sin\varphi_\ell, r_j\cos\varphi_\ell, z_p)^\top$,

$$\begin{aligned} z_p &= \frac{2p+1-P}{P}, && p = 0,\dots,P-1,\\ r_j &= \frac{j}{J}, && j = 0,\dots,J_p-1,\ J_p = \left\lfloor \sqrt{1-z_p^2}\cdot J \right\rfloor,\\ \varphi_\ell &= \frac{2\pi\ell}{N}, && \ell = 0,\dots,N-1, \end{aligned}$$

which leads to the discrete reconstruction formula

$$\begin{aligned} f_\varepsilon(x_{\ell,p,j}) \approx f_l^{j,p} &:= \frac{2(1-r_j^2-z_p^2)}{(I-1)MN}\sum_{m=0}^{M-1}\sum_{i=0}^{I-1}\sin\psi_{1,i} f_\ell^{j,m,p,i} \qquad (3.14)\\ f_\ell^{j,m,p,i} &:= \sum_{n=0}^{N-1} h_{n-l}^{j,m,p,i} g^{t_m,\psi_{1,i}}(\psi_{2,n})\\ h_r^{j,m,p,i} &:= h_{\varepsilon,q}(1+r_j^2+z_p^2-2z_p\cos\psi_{1,i}-t_m^2-2r_j\sin\psi_{1,i}\cos\psi_{2,r}). \end{aligned}$$

Using the idea of Algorithm 1 for each third spatial coordinate z_p individually, this approach is of particular interest if one needs to reconstruct f on a few horizontal planes only. For fixed j,m,p,i, the inner sum again is a discrete and cyclic convolution and realized by means of fast Fourier transforms in $\mathcal{O}(N\log N)$ floating point operations. Taking into account the outer summations over time and angle in (3.14) for all radii and angles, assuming that all discretization parameters are of order $\mathcal{O}(N)$, and considering the total problem size $n = N^3$ this leads to $\mathcal{O}(n^{5/3}\log n)$ floating point operations.

3.3. Generalizations. We note that the presented ideas can also be used for the ordinary Radon transform. Consider the classical Radon transform $\mathcal{M}f(\xi,s) = \int_{y\cdot\xi=s} f(y)\,\mathrm{d}y$ for $(\xi,s) \in \mathbb{S}^{d-1}\times\mathbb{R}$ and $d = 2,3$. An approximate reconstruction formula is given by

$$f_\varepsilon(x) = \frac{1}{\varepsilon^{d-1}}\int_{\mathbb{R}}\int_{\mathbb{S}^{d-1}} h\left(\frac{x\cdot\xi - s}{\varepsilon}\right)\mathcal{M}(\xi,t)\,\mathrm{d}\sigma(\xi)\,\mathrm{d}s, \qquad (3.15)$$

where we refer the reader to [15] for details and the corresponding choice of h. Again, expressing x,ξ in polar or spherical coordinates, respectively, results in a convolution type inner integral. Algorithms 1 and 2 can thus be used with few modifications for the efficient computation of (3.15).

In [1], the authors present an approximate reconstruction formula for more general geometries Ξ such as an ellipse. Thus one is also interested in a fast computation of integrals of the form

$$\int_0^\infty \int_\Xi h_\varepsilon(|x-\xi|^2 - t^2)\mathcal{R}(\xi,t)t^{d-1}\,\mathrm{d}\mu(\xi)\,\mathrm{d}t. \tag{3.16}$$

Unfortunately, the presented idea to rewrite the inner integral as a convolution is not possible in general, in particular fails if Ξ is an ellipse. However, certain lines, triangles, rectangles, etc. together with the shift invariant argument $|x-\xi|$ of h lead to a convolution type integral.

4. Numerical results. The implementation of Algorithm 1 and Algorithm 2 is realized in MATLAB and we use a Lenovo Thinkpad T60, 4GByte, Intel(R) Core(TM)2 Duo CPU P8700 2.53GHz for all numerical experiments. Besides introductory examples, our interest is the computation time for increasing discretization parameters and the accuracy with respect to the involved parameters.

4.1. Circular means. We start by some introductory example using the well known Shepp Logan phantom, see Figure 4.1(left). As for the ordinary Radon transform, its circular mean values can be computed analytically [6], Figure 4.1(middle & right) show the entire data and a profile for $\xi = (0,1)^\top$, respectively.

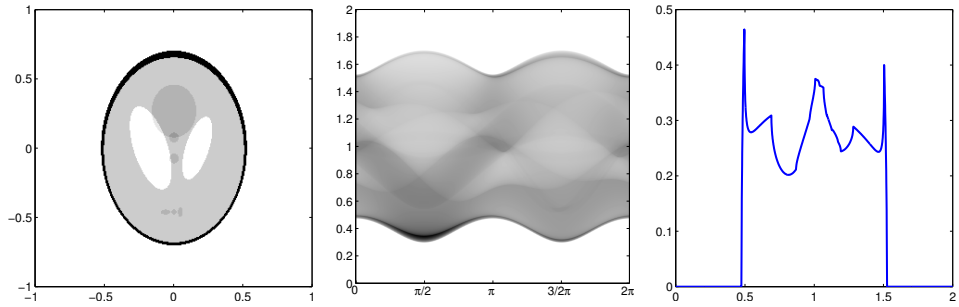

Fig. 4.1: Shepp Logan phantom (left) and circular mean values (middle) together with a profile for $\xi = (0,1)^\top$ (right).

The input of Algorithm 1 are these spherical means $\mathcal{R}f(\xi_n, t_m)$, $n = 0,\dots,N-1$, $m = 0,\dots,M-1$, for discretization parameters $N = 360$ and $M = 2000$. We reconstruct the phantom f on a polar grid with $J = 600$ radii and set the regularization parameter to $\varepsilon = 5\cdot 10^{-3}$. Figure 4.2(left & middle) shows the reconstruction on a Cartesian grid and a profile for $x_{(2)} = 0$, clearly visible is a smoothing effect on the jump singularities leading also to a damping of small details.

For the discussion of accuracy and computation time, we consider the function $f : \mathbb{R}^2 \to \mathbb{R}$,

$$f(x) = \left(1 - \frac{|x-a|^2}{0.6^2}\right)_+^3, \quad a = \frac{1}{5}(1,1)^\top,$$

We fix the regularization parameter $\varepsilon = 10^{-2}$, choose discretization parameters $N = M = J = 2^l$, $l = 1,\dots,12$, and interpolate to a Cartesian grid with $L = 2^{l-1}$

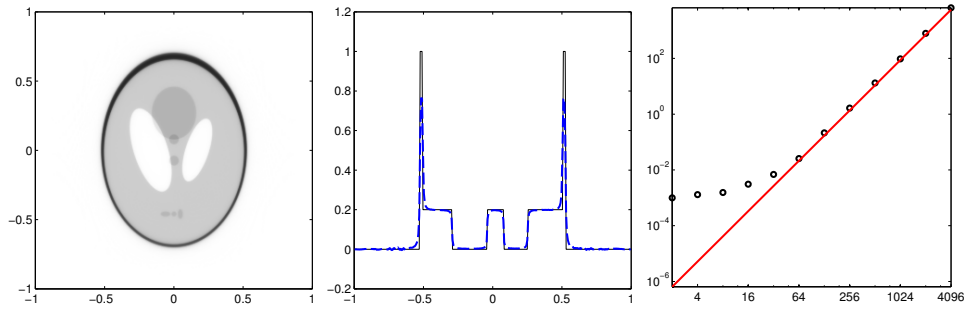

Fig. 4.2: Reconstruction of the Shepp Logan phantom, on a Cartesian grid (left) and a profile for $x_{(2)} = 0$ (middle). Computation times in seconds with respect to the common discretization parameter (right).

grid points in each coordinate, see Remark 2.1. Figure 4.2(right) shows the computation time for the reconstruction with interpolation together with the estimated order $\mathcal{O}\left(N^3\right)$, where we neglected the logarithmic term. The total accuracy of Algorithm 1 is measured by

$$E_\infty = \max_{\ell,j} |f(x_{\ell,j}) - f_l^j|, \tag{4.1}$$

and we consider this quantity for fixed parameters $N = J = 500$ and $M = 8000$ and a decreasing regularization parameter $\varepsilon = 2^{-l}$, $l = 1, \ldots, 10$. Table 4.1 shows an error behavior $E_\infty \approx 2.8\varepsilon$ until the discretization becomes too coarse at $\varepsilon \approx \frac{8}{M}$ resulting in an increasing error.

ε	2^{-1}	2^{-2}	2^{-3}	2^{-4}	2^{-5}
E_∞	$7.1 \cdot 10^{-1}$	$4.9 \cdot 10^{-1}$	$3.0 \cdot 10^{-1}$	$1.6 \cdot 10^{-1}$	$8.6 \cdot 10^{-2}$
ε	2^{-6}	2^{-7}	2^{-8}	2^{-9}	2^{-10}
E_∞	$4.4 \cdot 10^{-2}$	$2.2 \cdot 10^{-2}$	$1.1 \cdot 10^{-2}$	$5.7 \cdot 10^{-3}$	$4.9 \cdot 10^{-2}$

Table 4.1: Error of the reconstruction with respect to the regularization parameter.

4.2. Spherical means. We start again by some simple test-function as depicted in Figure 4.3(left). The spherical means of this superposition of characteristic functions of balls are computed analytically [6]. Figure 4.3(middle & right) show a equatorial cross section for $\xi_{(3)} = 0$ and a profile for $\xi = (1, 0, 0)^\top$ of these mean values, respectively.

The spherical means $\mathcal{R}f(\xi, t)$ are the input of Algorithm 2, they are given on a standard spherical grid $\xi_{i_1,i_2} = (\sin\psi_{i_1} \cos\varphi_{i_2}, \sin\psi_{i_1} \cos\varphi_{i_2}, \cos\psi_{i_1})^\top$, where

$$\psi_{i_1} = \frac{\pi i_1}{I_1} \qquad i_1 = 0, \ldots, I_1 - 1,$$
$$\varphi_{i_2} = \frac{2\pi i_2}{I_2} \qquad i_2 = 0, \ldots, I_2 - 1,$$

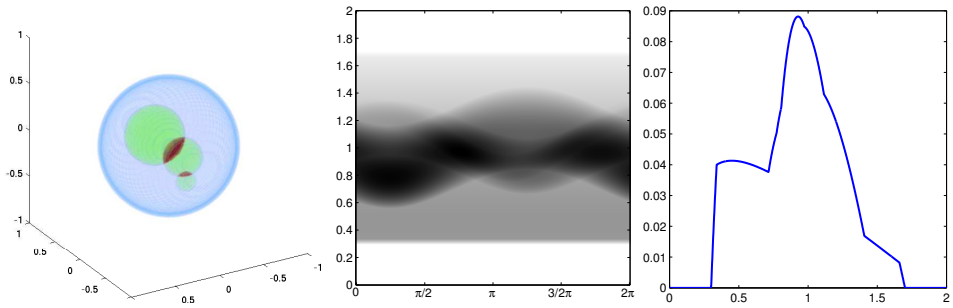

Fig. 4.3: Test-function (left) and spherical mean values values, the equatorial cross section for $\xi_{(3)} = 0$ (middle) and a profile for $\xi = (1, 0, 0)^\top$ (right).

$I = I_1 I_2$, and the discretization parameters are $I_1 = 100$, $I_2 = 200$, $M = 1500$. The remaining input parameters of Algorithm 2 are set as follows. We choose regularization parameters $q = 4$ and $\varepsilon = 4 \cdot 10^{-2}$, a cut-off degree $N = 100$, and reconstruct the test-function on a standard spherical grid $x_{j,i_1,i_2} = r_j \xi_{i_1,i_2}$ with $J = 200$ radii. The result after interpolating to a Cartesian grid and a profile for $x_{(2)} = x_{(3)} = 0$ are shown in Figure 4.4(left & middle).

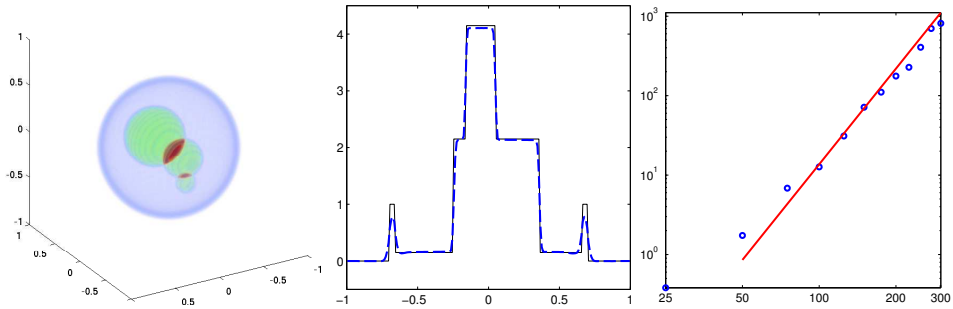

Fig. 4.4: Reconstruction on a Cartesian grid (left) and a profile (dashed together with the original function) for $x_{(2)} = x_{(3)} = 0$ (middle). Computation times in seconds ($\circ$) and estimated order $\mathcal{O}\left(N^4\right)$ with respect to the common discretization parameter N (right).

As for the two-dimensional case, we consider the function $f : \mathbb{R}^3 \to \mathbb{R}$,

$$f(x) = \left(1 - \frac{|x-a|^2}{0.6^2}\right)_+^3, \quad a = \frac{1}{5}(1,1,1)^\top,$$

for the discussion of the accuracy and computation time. Figure 4.4(right) shows the estimated arithmetic complexity $\mathcal{O}\left(N^4\right)$ and the actual time usage of Algorithm 2 for fixed regularization parameters $q = 4$, $\varepsilon = 10^{-2}$, and increasing discretization parameters $N = M = J = I_1 = I_2 = 25, 50, 75, \ldots, 300$.

Moreover, we consider the total accuracy (4.1) of Algorithm 2 with respect to the cut-off degree N and the regularization parameters ε, q. We fix the discretization

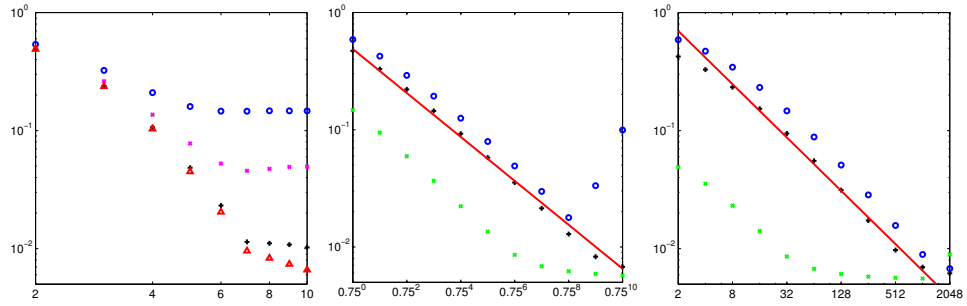

Fig. 4.5: Reconstruction error E_∞ with respect to the cut-off degree N (left) and the regularization parameters ε (middle) and q (right). In the left diagram, we fixed $q = 32$ and $\varepsilon = 1, 0.5, 0.75^6, 0.1$ ($\circ$, $\times$, $+$, $\triangle$). The second diagram shows E_∞ for fixed $N = 50$ and $q = 2, 4, 32$ ($\circ$, $+$, $\times$) together with the rate $\varepsilon^{3/2}$ (solid line). In the right diagram, we consider the error with respect to q and set $N = 50$ and $\varepsilon = 1, 0.75, 0.75^6$ ($\circ$, $+$, $\times$), in addition, the rate $q^{-3/4}$ is shown (solid line).

parameters $I_1 = 100$, $I_2 = 200$, $J = 100$, and $M = 2000$. Figure 4.5(left) shows the reconstruction error for fixed regularization parameters $q = 32$, $\varepsilon = 1, 0.5, 0.75^6, 0.1$, and increasing cut-off degree $N = 2, \ldots, 10$. Surprisingly, already a small cut-off degree $N = 10$ achieves an accuracy smaller than 10^{-2} for $\varepsilon = 0.75^6, 0.1$ and we thus fix the cut-off degree $N = 50$ subsequently. Figure 4.5(middle) shows the reconstruction error for decreasing regularization parameter $\varepsilon = 0.75^l$, $l = 0, \ldots, 10$ and fixed $q = 2, 4, 32$. Up to the finally achieved accuracy, depending mainly on the time discretization M, the error decays at a rate $\varepsilon^{3/2}$. Finally, we consider E_∞ with respect to the regularization parameter $q = 2^l$, $l = 1, \ldots, 11$, and for fixed $N = 50$ and $\varepsilon = 1, 0.75, 0.75^6$ in Figure 4.5(right). Here, the numerical error decays at a rate $q^{-3/4}$.

5. Summary. We suggested effective discretizations for the recovery of a function from its spherical means in spherical acquisition geometry. For a total problem size n, the resulting algorithms have complexity $\mathcal{O}(n^{\frac{3}{2}} \log n)$ and $\mathcal{O}(n^{\frac{4}{3}})$ for the two- and three-dimensional case, respectively. While this is still slower than the efficient schemes [14] for *exact* reconstruction formulas, it improves over the best known results [11] for *approximate* inversion.

Acknowledgment. The authors thank the referees for their valuable suggestions and gratefully acknowledge support by the German Research Foundation within the project KU 2557/1-1 and by the Helmholtz Association within the young investigator group VH-NG-526.

REFERENCES

[1] M. Ansorg, F. Filbir, W. R. Madych, and R. Seyfried. Summability kernels for circular and spherical mean data. *Inverse Problems*, 29(1):015002, 2013.

[2] V. A. Antonov, K. V. Kholshevnikov, and V. S. Shaidulin. Estimating the derivative of the Legendre polynomial. *Vestnik St. Petersburg Univ. Math.*, 43(4):191–197, 2010.

[3] F. Filbir, R. Hielscher, and W. R. Madych. Reconstruction from circular and spherical mean data. *Appl. Comput. Harmon. Anal.*, 29(1):111–120, 2010.

[4] D. Finch, M. Haltmeier, and Rakesh. Inversion of spherical means and the wave equation in even dimensions. *SIAM J. Appl. Math.*, 68(2):392–412, 2007.

[5] D. Finch, S. K. Patch, and Rakesh. Determining a function from its mean values over a family of spheres. *SIAM J. Math. Anal.*, 35(5):1213–1240, 2004.

[6] T. Görner and S. Kunis. SMV, Matlab toolbox for computing spherical mean values. `http://www.analysis.uos.de/software`, 2012.

[7] M. Gräf, S. Kunis, and D. Potts. On the computation of nonnegative quadrature weights on the sphere. *Appl. Comput. Harmon. Anal.*, 27:124 – 132, 2009.

[8] M. Haltmeier. A mollification approach for inverting the spherical mean Radon transform. *SIAM J. Appl. Math.*, 71(5):1637–1652, 2011.

[9] M. Haltmeier. Inversion of circular means and the wave equation on convex planar domains. *Comput. Math. Appl.*, 65(7), 2013.

[10] M. Haltmeier. Universal inversion formulas for recovering a function from spherical means. *SIAM J. Math. Anal.*, 46(1):214–232, 2014.

[11] M. Haltmeier, T. Schuster, and O. Scherzer. Filtered backprojection for thermoacoustic computed tomography in spherical geometry. *Math. Methods Appl. Sci.*, 28(16):1919–1937, 2005.

[12] J. Keiner, S. Kunis, and D. Potts. Fast summation of radial functions on the sphere. *Computing*, 78(1):1 – 15, 2006.

[13] J. Keiner, S. Kunis, and D. Potts. Using NFFT 3—a software library for various nonequispaced fast Fourier transforms. *ACM Trans. Math. Software*, 36(4):Art. 19, 30, 2009.

[14] L. Kunyansky. Fast reconstruction algorithms for the thermoacoustic tomography in certain domains with cylindrical or spherical symmetries. *Inverse Probl. Imaging*, 6(1):111–131, 2012.

[15] W. R. Madych. Summability and approximate reconstruction from Radon transform data. In *Integral geometry and tomography (Arcata, CA, 1989)*, volume 113 of *Contemp. Math.*, pages 189–219. Amer. Math. Soc., Providence, RI, 1990.

[16] V. P. Palamodov. A uniform reconstruction formula in integral geometry. *Inverse Problems*, 28(6):065014, 15, 2012.

[17] R. Seyfried. Summability methods for the inversion of the spherical mean operator. PhD thesis, Osnabrück University. `http://www.helmholtz-muenchen.de/fileadmin/ICB/mathematical-imaging-and-data-analysis/DissSeyfried.pdf`, 2014.

[18] G. Szegő. *Orthogonal polynomials*. American Mathematical Society, Providence, R.I., fourth edition, 1975. American Mathematical Society, Colloquium Publications, Vol. XXIII.

[19] L. N. Trefethen and J. A. C. Weideman. The exponentially convergent trapezoidal rule. *SIAM Rev.*, to appear.